



4th Int. Workshop on High-Order CFD Methods, Crete Island, Greece, June 4th-5th, 2016

Computational/Meshing Challenge C1 - DLR F11

Results based on CENTAUR and the DLR-PADGE code

Ralf Hartmann¹, Harlan McMorris², Tobias Leicht¹

¹DLR (German Aerospace Center), Institute of Aerodynamics and Flow Technology, Braunschweig

²CentauroSoft, Austin, TX

5. June 2016



Deutsches Zentrum
für Luft- und Raumfahrt e.V.
in der Helmholtz-Gemeinschaft

AR1 RANS of the Common Research Model
Results of the DLR-PADGE code
Ralf Hartmann, Harlan McMorris, Tobias Leicht

Computational/Meshing Challenge C1 - DLR F11

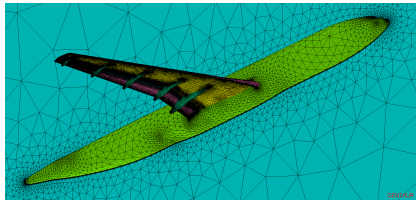
Meshing challenge:

- ▶ Quadratic hybrid/mixed-element meshes by the CENTAUR grid generator

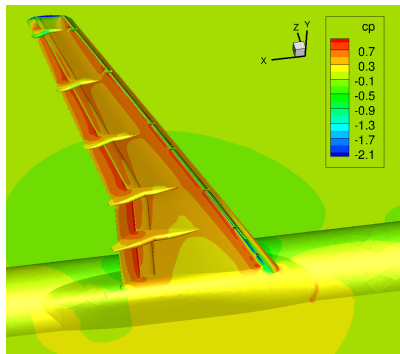
Computational challenge:

- ▶ Stabilized DG discretization and implicit solver in the DLR-PADGE code

DLR-F11 high-lift configuration
with slat tracks and flap track fairings



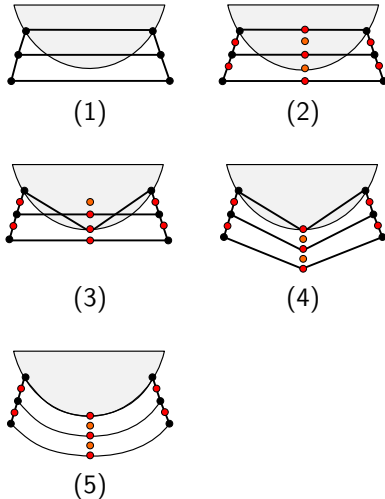
hybrid/mixed-element 3rd-order grid



3rd-order flow solution

Linear and quadratic mesh generation process (CENTAUR)

- (1) Generate a coarse, linear hybrid grid.
- (2) Insert an additional midpoint for every grid edge and quadrilateral face.
- (3) Use the CAD information to map each new boundary point onto the underlying CAD surface.
- (4) Adjust the position of the interior points based on the mapped position of the boundary edge midpoints, in order to prevent self-intersecting grid elements and to ensure grid validity.
- (5) Quadratic interpolation of points and interior points for a curved element representation.



Linear and quadratic mesh generation process (CENTAUR)

For the grid generation of a particularly coarse linear mesh

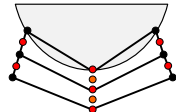
- ▶ a lower analytic curvature clustering, and
- ▶ a larger maximum element size

are used than for linear meshes typically generated for 2nd order schemes.

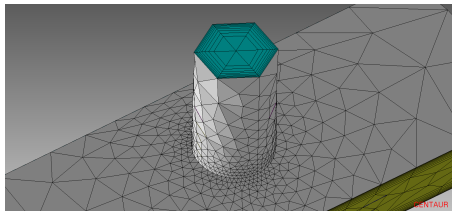
After curving of the mesh the grid quality is evaluated using

- ▶ the volumes, and the
- ▶ the volume ratios

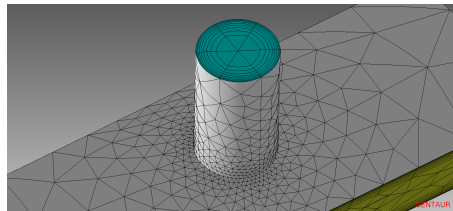
of the complete elements and sub-elements.



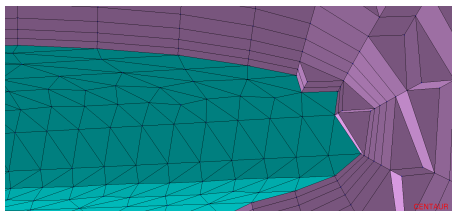
Linear and quadratic mesh generation process: Examples



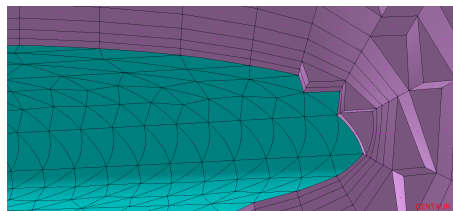
linear mesh



quadratic mesh



linear mesh



quadratic mesh

Linear and quadratic mesh generation: Application to DLR-F11

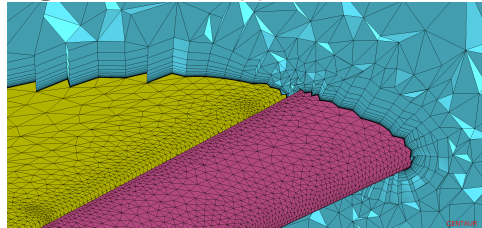
Coarse mesh with

2 365 919 prisms

42 603 pyramids

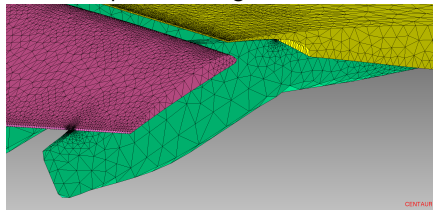
1 116 213 tetrahedra

3 524 735 elements

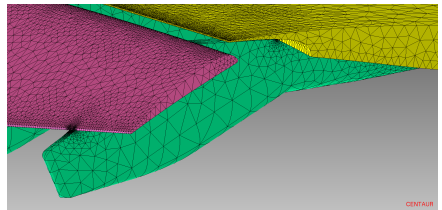


prism layers around the slat and leading edge of the main

Outboard flap track fairing surface mesh:



linear mesh



quadratic mesh

Linear and quadratic mesh generation: Application to DLR-F11

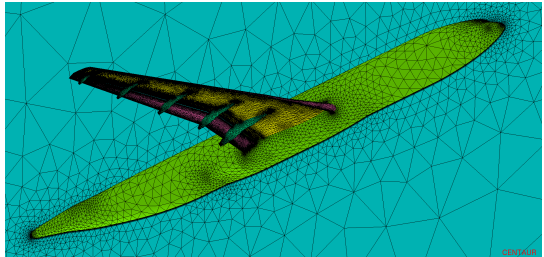
Coarse mesh with

2 365 919 prisms

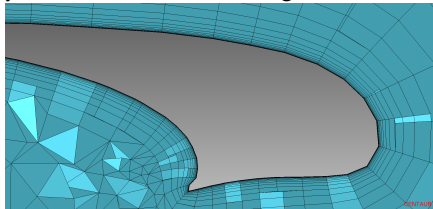
42 603 pyramids

1 116 213 tetrahedra

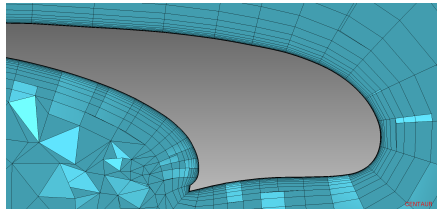
3 524 735 elements



Hybrid mesh cuts in the slat region:



linear mesh



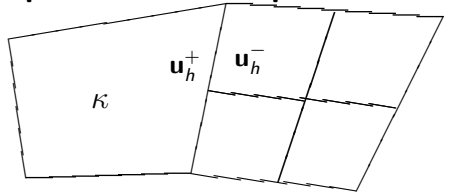
quadratic mesh

The DG discretization of the compressible Euler equations

The problem:

$$\nabla \cdot \mathcal{F}^c(\mathbf{u}) = 0 \quad \text{in } \Omega \subset \mathbb{R}^2,$$

with $\mathbf{u} = (\varrho, \varrho v_1, \varrho v_2, \varrho E)^T$.



The DG(p) discretization: Find \mathbf{u}_h in \mathbf{V}_h^p such that

$$\begin{aligned} N_h(\mathbf{u}_h, \mathbf{v}_h) &\equiv \sum_{\kappa \in \mathcal{T}_h} \left\{ - \int_{\kappa} \mathcal{F}^c(\mathbf{u}_h) : \nabla \mathbf{v}_h \, d\mathbf{x} + \int_{\partial \kappa \setminus \Gamma} \hat{\mathbf{h}}(\mathbf{u}_h^+, \mathbf{u}_h^-, \mathbf{n}) \cdot \mathbf{v}_h^+ \, ds \right\} \\ &\quad + \int_{\Gamma} \hat{\mathbf{h}}_{\Gamma}(\mathbf{u}_h^+, \mathbf{n}) \cdot \mathbf{v}_h^+ \, ds = 0 \quad \forall \mathbf{v}_h \in \mathbf{V}_h^p, \end{aligned}$$

Numerical flux function $\hat{\mathbf{h}}$: Roe flux, local Lax-Friedrichs flux, ...

Numerical flux function $\hat{\mathbf{h}}_{\Gamma}$ at the boundary:

- ▶ $\hat{\mathbf{h}}_{\Gamma}(\mathbf{u}_h^+, \mathbf{n}) = \mathbf{n} \cdot \mathcal{F}^c(\mathbf{u}_{\Gamma}(\mathbf{u}_h^+))$ allows for an adjoint consistent discretization
- ▶ $\hat{\mathbf{h}}_{\Gamma}(\mathbf{u}_h^+, \mathbf{n}) = \hat{\mathbf{h}}(\mathbf{u}_h^+, \mathbf{u}_{\Gamma}^*(\mathbf{u}_h^+), \mathbf{n})$ is, to our experience, significantly more stable

Numerical flux function at the boundary

Use the same numerical flux on the boundary like on interior faces

$$\hat{\mathbf{h}}_{\Gamma,h} = \hat{\mathbf{h}}_{\Gamma}(\mathbf{u}_h^+, \mathbf{n}) = \hat{\mathbf{h}}(\mathbf{u}_h^+, \mathbf{u}_{\Gamma}^-(\mathbf{u}_h^+), \mathbf{n}),$$

where the *boundary exterior state* $\mathbf{u}_{\Gamma}^-(\mathbf{u}_h^+)$ is computed from

$\frac{1}{2} (\mathbf{u}_h^+ + \mathbf{u}_{\Gamma}^-(\mathbf{u}_h^+)) = \mathbf{u}_{\Gamma}(\mathbf{u}_h^+)$ with $\mathbf{n} \cdot \mathbf{v}_{\Gamma} = 0$, the discretization is given by

$$-\int_{\Omega} \mathcal{F}^c(\mathbf{u}_h) : \nabla_h \mathbf{v}_h \, d\mathbf{x} + \sum_{\kappa \in \mathcal{T}_h} \int_{\partial\kappa \setminus \Gamma} \hat{\mathbf{h}}_h \cdot \mathbf{v}_h^+ \, ds + \int_{\Gamma} \hat{\mathbf{h}}(\mathbf{u}_h^+, \mathbf{u}_{\Gamma}^-(\mathbf{u}_h^+), \mathbf{n}) \cdot \mathbf{v}_h^+ \, ds = 0.$$

This discretization is **adjoint inconsistent** in combination with both

$$J_h(\mathbf{u}_h) = \int_{\Gamma_W} p(\mathbf{u}_{\Gamma}(\mathbf{u}_h^+)) \, \mathbf{n} \cdot \boldsymbol{\psi} \, ds = J(\mathbf{u}_{\Gamma}(\mathbf{u}_h^+)),$$

and

$$J(\mathbf{u}_h) = \int_{\Gamma_W} p(\mathbf{u}_h) \, \mathbf{n} \cdot \boldsymbol{\psi} \, ds.$$

Adjoint consistent discretization of force coefficients

Consider the discretization: find \mathbf{u}_h in \mathbf{V}_h^P such that

$$-\int_{\Omega} \mathcal{F}^c(\mathbf{u}_h) : \nabla \mathbf{v}_h \, d\mathbf{x} + \sum_{\kappa \in \mathcal{T}_h} \int_{\partial\kappa \setminus \Gamma} \hat{\mathbf{h}}_h \cdot \mathbf{v}_h^+ \, ds + \int_{\Gamma} \hat{\mathbf{h}}_{\Gamma,h} \cdot \mathbf{v}_h^+ \, ds = 0 \quad \mathbf{v}_h \in \mathbf{V}_h^P \quad (1)$$

Consider the target quantity and its discretization

$$J(\mathbf{u}) = \int_{\Gamma_W} p(\mathbf{u}) \mathbf{n} \cdot \psi \, ds, \quad J_h(\mathbf{u}_h) = \int_{\Gamma_W} \hat{\mathbf{h}}_{\Gamma,h} \cdot \tilde{\psi} \, ds, \quad (2)$$

with $\tilde{\psi} = (0, \psi_1, \psi_2, 0)^\top$ for $\psi = (\psi_1, \psi_2)^\top$, and

$$\hat{\mathbf{h}}_{\Gamma,h} = \hat{\mathbf{h}}_\Gamma(\mathbf{u}_h^+, \mathbf{n}) = \hat{\mathbf{h}}(\mathbf{u}_h^+, \mathbf{u}_\Gamma^-(\mathbf{u}_h^+), \mathbf{n}),$$

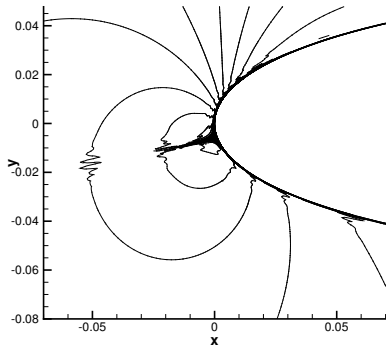
It can be shown¹, that (1) in combination with (2) is **adjoint consistent**.

¹R. Hartmann and T. Leicht. Generalized adjoint consistent treatment of wall boundary conditions for compressible flows, J. Comput. Phys., 300: 754-778, 2015.

Example: Inviscid flow around the NACA0012 airfoil

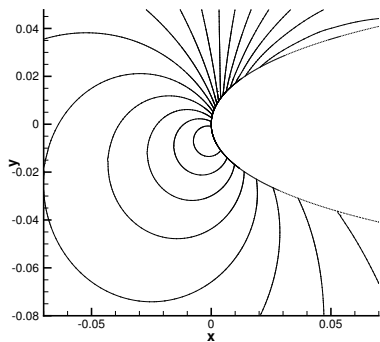
$M = 0.5, \alpha = 2^\circ$, numerical flux at the wall boundary: $\hat{h}_{\Gamma,h} = \hat{h}(u_h^+, u_\Gamma^-(u_h^+), n)$

z_1 isolines of the discrete adjoint solution z_h for C_{dp} :



$$J_h(u_h) = J(u_\Gamma(u_h^+))$$

adjoint inconsistent



$$J_h(u_h) = \int_{\Gamma_W} \hat{h}_{\Gamma,h} \cdot \tilde{\psi} \, ds$$

adjoint consistent

Extension to viscous flows

$$\int_{\Omega} (-\mathcal{F}^c(\mathbf{u}_h) + \mathcal{F}^v(\mathbf{u}_h, \nabla_h \mathbf{u}_h)) : \nabla_h \mathbf{v}_h \, d\mathbf{x} + \dots + \int_{\Gamma} (\hat{\mathbf{h}}_{\Gamma,h} - \hat{\sigma}_{\Gamma,h} \mathbf{n}) \cdot \mathbf{v}_h \, ds$$

is **adjoint consistent** in combination with

$$J(\mathbf{u}) = \int_{\Gamma_W} (p \mathbf{n} - \underline{\tau} \mathbf{n}) \cdot \psi \, ds, \quad J_h(\mathbf{u}_h) = \int_{\Gamma_W} (\hat{\mathbf{h}}_{\Gamma,h} - \hat{\sigma}_{\Gamma,h} \mathbf{n}) \cdot \tilde{\psi} \, ds,$$

with $\tilde{\psi} = (0, \psi_1, \psi_2, 0)^{\top}$ for $\psi = (\psi_1, \psi_2)^{\top}$.

Adjoint consistent treatment of integral and local quantities

Discretization of flow equations:

$$\int_{\Omega} (-\mathcal{F}^c(\mathbf{u}_h) + \mathcal{F}^v(\mathbf{u}_h, \nabla_h \mathbf{u}_h)) : \nabla_h \mathbf{v}_h \, d\mathbf{x} + \dots + \int_{\Gamma} (\hat{\mathbf{h}}_{\Gamma,h} - \underline{\hat{\sigma}}_{\Gamma,h} \mathbf{n}) \cdot \mathbf{v}_h \, ds$$

Adjoint consistent discretization of **integral** quantities (drag, lift coefficients):

$$J(\mathbf{u}) = \int_{\Gamma_W} (\rho \mathbf{n} - \underline{\tau} \mathbf{n}) \cdot \psi \, ds, \quad J_h(\mathbf{u}_h) = \int_{\Gamma_W} (\hat{\mathbf{h}}_{\Gamma,h} - \underline{\hat{\sigma}}_{\Gamma,h} \mathbf{n}) \cdot \tilde{\psi} \, ds.$$

Adjoint consistent discretization of **local** quantities (surface pressure, skin friction):

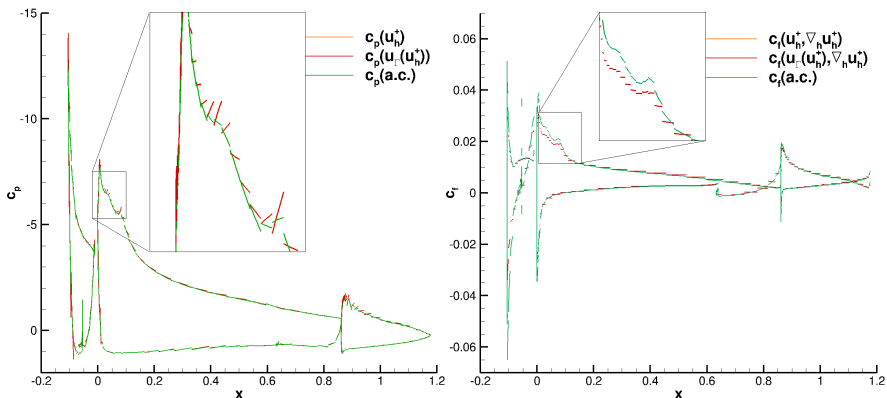
$$\begin{aligned} c_p(\mathbf{u}) &= \frac{p(\mathbf{u}) - p_{\infty}}{\frac{1}{2} \rho_{\infty} v_{\infty}^2}, & c_{p,h}(\mathbf{u}_h) &= \frac{\hat{\mathbf{h}}_{\Gamma,h} \cdot \tilde{\mathbf{n}} - p_{\infty}}{\frac{1}{2} \rho_{\infty} v_{\infty}^2}, \\ c_f(\mathbf{u}, \nabla \mathbf{u}) &= \frac{\tau_w(\mathbf{u}, \nabla \mathbf{u})}{\frac{1}{2} \rho_{\infty} v_{\infty}^2}, & c_{f,h}(\mathbf{u}_h, \nabla \mathbf{u}_h) &= -\frac{(\underline{\hat{\sigma}}_{\Gamma,h} \mathbf{n}) \cdot \tilde{\mathbf{t}}}{\frac{1}{2} \rho_{\infty} v_{\infty}^2}, \end{aligned}$$

with $\tilde{\mathbf{n}} = (0, n_1, n_2, 0)^T$ for the normal vector $\mathbf{n} = (n_1, n_2)^T$,
and $\tilde{\mathbf{t}} = (0, t_1, t_2, 0)^T$ for the tangential vector $\mathbf{t} = (t_1, t_2)^T$.

Example: L1T2 high-lift configuration

RANS & Wilcox $k-\omega$ model, $M = 0.197$, $\alpha = 20.18^\circ$, $Re = 3.52 \times 10^6$

$$\hat{\mathbf{h}}_{\Gamma,h} = \hat{\mathbf{h}}_{\Gamma}(\mathbf{u}_h^+, \mathbf{n}) = \hat{\mathbf{h}}(\mathbf{u}_h^+, \mathbf{u}_{\Gamma}^-(\mathbf{u}_h^+), \mathbf{n}).$$



c_p - and c_f -distributions of the $p = 1$ flow solution

Regularity check of a curved mesh

Discrete regularity check:

- ▶ Consider the mapping σ from the reference element $\hat{\kappa}$ to the element κ in physical space. The determinant of its Jacobian matrix $\frac{d\sigma}{dx}$ is required in numerical quadrature:

$$|\kappa| = \int_{\hat{\kappa}} \det(J) dx \approx \sum_q \det(J(\hat{x}_q)) w_q$$

- ▶ Check whether the Jacobian determinants $\det(J(\hat{x}_q))$ are positive in each of the quadrature points.

Note,

- ▶ that this discrete regularity check checks *necessary* conditions only,
- ▶ whereas the check based on Bézier functions¹ would give a *necessary and sufficient* condition for validity.

¹A. Johnen, J.-F. Remacle, and C. Geuzaine. Geometrical validity of curvilinear finite elements. *J. Comput. Phys.*, 233:359–272, 2013.

Regularity check of the quadratic DLR-F11 mesh

$$|\kappa| = \int_{\hat{\kappa}} \det(J) \, d\mathbf{x} \approx \sum_q \det(J(\mathbf{x}_q)) w_q$$

Discrete regularity check: $\det(J(\mathbf{x}_q)) > 0$ for all quadrature points \mathbf{x}_q ?

“Discrete regularity” check of the quadratic mesh around the DLR-F11 mesh with 3 524 735 curved elements (prisms, pyramids and tetrahedras):

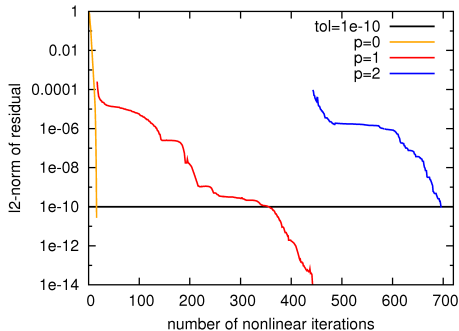
degree	# DoFs/eqn	# quadrature points/elem.	# irregular elements	worst # neg. Jac./element
0	3 524 735	8	0	0/8
1	14 098 940	27	0	0/27
2	35 247 350	64	14	2/64

Application to the DLR-F11 (Config 4): The solution process

RANS & Wilcox $k-\omega$ model, flow conditions: $M = 0.175$, $Re = 15.1 \cdot 10^6$, $\alpha = 7^\circ$
Flow solver:

- ▶ Fully implicit (Backward-Euler) solver
- ▶ Convergence criterion: nonlinear residual below 10^{-10} .
- ▶ Linear systems solved with GMRes and ILU per process
- ▶ The CFL number is increased as the nonlinear residual decreases
- ▶ Diverging steps are recomputed with CFL/2.

Numerical boundary flux: $\hat{\mathbf{h}}_\Gamma = \hat{\mathbf{h}}(\mathbf{u}_h^+, \mathbf{u}_\Gamma^-(\mathbf{u}_h^+), \mathbf{n})$.

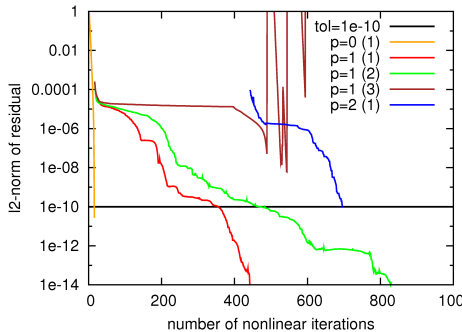


degree	# DoFs/eqn	res tol	start CFL	end CFL	steps lost
0	3.5e6	10^{-10}	100	120 000	0/16
1	14.1e6	10^{-10}	5	500	45/339
		$\dots 10^{-14}$			+18/87
2	35.2e6	10^{-10}	10	200	24/254

Application to the DLR-F11 (Config 4): The solution process

RANS & Wilcox $k-\omega$ model, flow conditions: $M = 0.175$, $Re = 15.1 \cdot 10^6$, $\alpha = 7^\circ$
Flow solver:

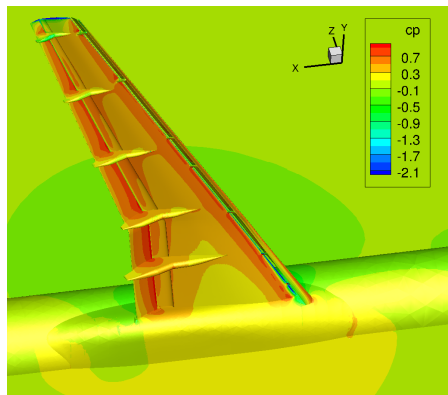
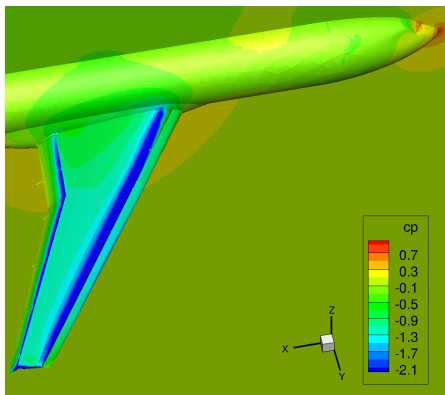
- ▶ Fully implicit (Backward-Euler) solver
- ▶ Convergence criterion: nonlinear residual below 10^{-10} .
- ▶ Linear systems solved with GMRes and ILU per process
- ▶ The CFL number is increased as the nonlinear residual decreases



legend	numerical flux	recompute diverging steps with CFL/2
p=1 (1)	$\hat{h}(\mathbf{u}_h^+, \mathbf{u}_\Gamma^-(\mathbf{u}_h^+), \mathbf{n})$	yes
p=1 (2)	$\mathbf{n} \cdot \mathcal{F}^c(\mathbf{u}_\Gamma(\mathbf{u}_h^+))$	yes
p=1 (3)	$\mathbf{n} \cdot \mathcal{F}^c(\mathbf{u}_\Gamma(\mathbf{u}_h^+))$	no

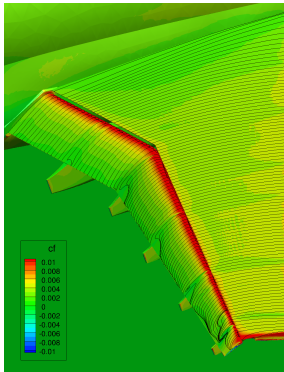
DLR-F11 high lift configuration: The flow solution

RANS & Wilcox $k-\omega$ model, flow conditions: $M = 0.175$, $Re = 15.1 \cdot 10^6$, $\alpha = 7^\circ$.
3rd-order solution on the quadratic (3rd-order) mesh:

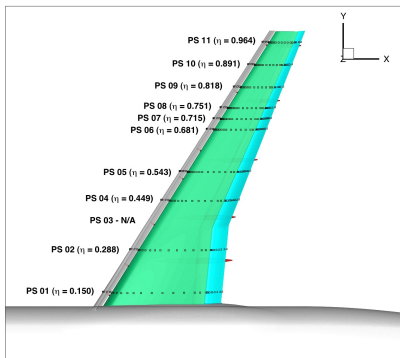


DLR-F11 high lift configuration: The flow solution

RANS & Wilcox $k-\omega$ model, flow conditions: $M = 0.175$, $Re = 15.1 \cdot 10^6$, $\alpha = 7^\circ$.
3rd-order solution on the quadratic (3rd-order) mesh:

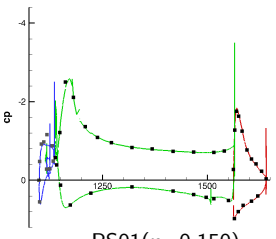


separation above flap track
fairings and at wing tip

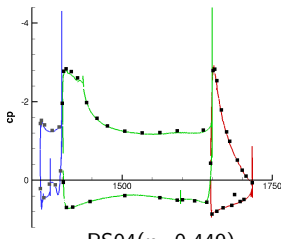


consider pressure tab locations 01, 04, 06, 10

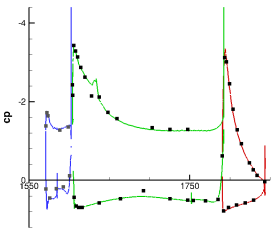
DLR-F11 high lift configuration: The flow solution



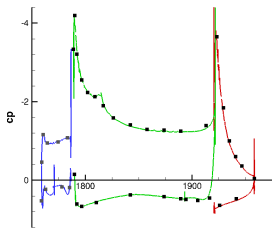
PS01($\eta = 0.150$)



PS04($\eta = 0.449$)



PS06($\eta = 0.681$)



PS10($\eta = 0.891$)

RANS & Wilcox
 $k-\omega$ model
 $M = 0.175$
 $Re = 15.1 \cdot 10^6$
 $\alpha = 7^\circ$

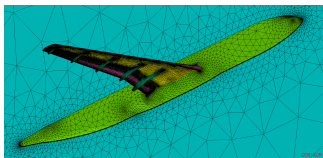
3rd-order
solution on
3rd-order mesh

	C_L	C_D	C_M
Exp.	1.927	0.162	-0.539
TAU	1.879	0.168	-0.565
	-2.5%	+4.1%	-4.8%
DG-O3	1.878	0.165	-0.570
	-2.5%	+2.1%	-5.8%

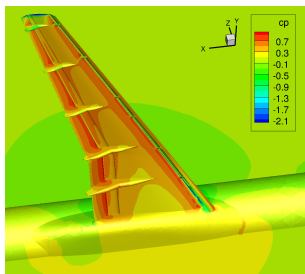
Computational/Meshing Challenge C1 - DLR F11

- ▶ Quadratic hybrid/mixed-element mesh by the CENTAUR grid generator.
- ▶ Stabilized DG discretization and solver in the DLR-PADGE code:
 - ▶ For stability use interior flux also on the boundary. For adjoint consistency use the same flux also
 - ▶ for the evaluation of integral quantities (force coefficients), and
 - ▶ for an according evaluation of local quantities (c_p - and c_f -distributions)
 - ▶ Recompute diverging solver steps with CFL/2.

DLR-F11 high-lift configuration
with slat tracks and flap track fairings



hybrid/mixed-element 3rd-order grid



3rd-order flow solution